J|A|C|S ARTICLES

Published on Web 08/10/2009

Correlating Particle Size and Shape of Supported Ru/γ-Al_2O_3 Catalysts with NH_3 Decomposition Activity

Ayman M. Karim,[†,§] Vinay Prasad,[†,⊥] Giannis Mpourmpakis,[†] William W. Lonergan,[†] Anatoly I. Frenkel,[‡] Jingguang G. Chen,[†] and Dionisios G. Vlachos*[,†]

Department of Chemical Engineering and Center for Catalytic Science and Technology, University of Delaware, Newark, Delaware 19716, and Department of Physics, Yeshiva University, New York, New York 10016

Received April 1, 2009; E-mail: vlachos@udel.edu

Abstract: While ammonia synthesis and decomposition on Ru are known to be structure-sensitive reactions, the effect of particle shape on controlling the particle size giving maximum turnover frequency (TOF) is not understood. By controlling the catalyst pretreatment conditions, we have varied the particle size and shape of supported Ru/γ-Al_2O_3 catalysts. The Ru particle shape was reconstructed by combining microscopy, chemisorption, and extended X-ray absorption fine structure (EXAFS) techniques. We show that the particle shape can change from a round one, for smaller particles, to an elongated, flat one, for larger particles, with suitable pretreatment. Density functional theory calculations suggest that the calcination most likely leads to planar structures. We show for the first time that the number of active (here B_5) sites is highly dependent on particle shape and increases with particle size up to 7 nm for flat nanoparticles. The maximum TOF (based on total exposed Ru atoms) and number of active (B_5) sites occur at ~7 nm for elongated nanoparticles compared to at ~1.8−3 nm for hemispherical nanoparticles. A complete, first-principles based microkinetic model is constructed that can quantitatively describe for the first time the effect of varying particle size and shape on Ru activity and provide further support of the characterization results. In very small nanoparticles, particle size polydispersity (due to the presence of larger particles) appears to be responsible for the observed activity.

1. Introduction

There has been an increasing interest in ammonia decomposition as a CO-free source of hydrogen for fuel cells. In addition, ammonia is a good hydrogen storage material since it liquefies at relatively low pressures (at room temperature) and has a high hydrogen storage capacity (>17 wt %), and its synthesis is a fairly mature and widespread technology.[1−3] The best single metal catalyst for this reaction is Ru. Due to the high cost of Ru, increasing the catalyst activity via particle size and shape control is of both fundamental and practical importance.

NH_3 synthesis and decomposition on Ru have been known to be structure-sensitive reactions.[4−11] This sensitivity stems from the chemistry happening primarily on B_5-type step (active) sites.[8,12] Yet, limited direct information exists on the effects of particle size, shape, and catalyst precursor on catalyst activity. In most previous reports, the size for maximum turnover frequency (TOF) was estimated theoretically to be in the range of 1.8−2.5 nm,[6,8,12] often assuming a hexagonal shape (independent of size) exposing only the (001) and (100) surfaces.[8] More recently, Gavnholt and Schiøtz predicted the optimal Ru particle size to be ~3 nm via energy minimization of particle shapes consisting of (001), (101), and (100) surfaces.[12] These theoretical estimates do not account for the interaction of Ru with the support, and the possibility of the particle shape varying with size and catalyst pretreatment. Aside from theoretical estimates, there have been a limited number of experimental studies on the effect of Ru particle size on Ru activity in ammonia synthesis and decomposition. The activity of Ru/C for ammonia synthesis was reported to increase with increasing particle size up to 4 nm, above which the TOF reached a plateau,[6] with the authors attributing this increase to promoters Ba and Cs. Other studies either did not examine particle sizes

[†] University of Delaware.
[‡] Yeshiva University.
[§] Current address: Institute for Interfacial Catalysis, Pacific Northwest National Laboratory, PO Box 999, Richland, WA 99354.
[⊥] Current address: Department of Chemical and Materials Engineering, University of Alberta, Edmonton, Alberta T6G 2V4, Canada.

(1) Rosowski, F.; Hornung, A.; Hinrichsen, O.; Herein, D.; Muhler, M.; Ertl, G. *Appl. Catal., A* **1997**, *151*, 443–460.
(2) Loffler, D. G.; Schmidt, L. D. *J. Catal.* **1976**, *59*, 195–204.
(3) Satterfield, C. N. *Heterogeneous Catalysis in Industrial Practice*, 2nd ed.; McGraw-Hill, Inc.: New York, 1991.
(4) Egawa, C.; Nishida, T.; Naito, S.; Tamaru, K. *J. Chem. Soc., Faraday Trans. I* **1984**, *80*, 1595–1604.
(5) Rarog-Pilecka, W.; Smigiel, D.; Komornicki, A.; Zielinski, J.; Kowalczyk, Z. *Carbon* **2003**, *41*, 589–591.
(6) Rarog-Pilecka, W.; Miskiewicz, E.; Szmigiel, D.; Kowalczyk, Z. *J. Catal.* **2005**, *231*, 11–19.
(7) Rossetti, I.; Forni, L. *Appl. Catal., A* **2005**, *282*, 315–320.
(8) Jacobsen, C. J. H.; Dahl, S.; Hansen, P. L.; Tornqvist, E.; Jensen, L.; Topsoe, H.; Prip, D. V.; Moenshaug, P. B.; Chorkendorff, I. *J. Mol. Catal A: Chem.* **2000**, *163*, 19–26.
(9) Zheng, W. Q.; Zhang, J.; Xu, H. Y.; Li, W. Z. *Catal. Lett.* **2007**, *119*, 311–318.
(10) Song, Z.; Cai, T.; Hanson, J. C.; Rodriguez, J. A.; Hrbek, J. *J. Am. Chem. Soc.* **2004**, *126*, 8576–8584.
(11) Dahl, S.; Törnqvist, E.; Chorkendorff, I. *J. Catal.* **2000**, *192*, 381–390.
(12) Gavnholt, J.; Schiøtz, J. *Phys. Rev. B* **2008**, *77*, 035404.

10.1021/ja902587k CCC: $40.75

above 3 nm[8] or did not compare the activity of different particle sizes resulting from different Ru precursors and/or catalyst supports.[5] Zheng et al. varied the particle size of Ru/Al_2O_3 by varying the Ru loading, and while they claimed the highest TOF for ammonia decomposition at a particle size of 2.2 nm,[9] their data did not support their conclusions. To our knowledge, there has not been a study in which the Ru particle size has been varied over a large range. In addition, the effect of Ru particle shape on activity has not been addressed. Furthermore, structural characterization of Ru catalysts has typically been limited either to transmission electron microscopy (TEM)[8,13] or chemisorption,[8] but often not simultaneously. Atomic level structural characterization and particle shape reconstruction has not been reported previously.

In this work, we synthesized $Ru/\gamma\text{-}Al_2O_3$ catalysts from two catalyst precursors with different average Ru particle sizes, ranging from 0.8 to 7.5 nm. We show that catalyst pretreatment (and not the Ru precursor) has a strong effect on Ru average particle size as well as particle shape. Particle size and shape reconstruction were performed for the first time via simultaneous TEM, CO chemisorption, and extended X-ray absorption fine structure (EXAFS) techniques. Density functional theory (DFT) calculations are performed to obtain insights into the mechanism responsible for the structures determined experimentally. The TOF of NH_3 decomposition increases by almost 2 orders of magnitude when increasing the Ru particle size from 0.8 to 7.5 nm. A first-principles based microkinetic model is constructed and found to describe data quantitatively while confirming insights obtained from the characterization results. The effect of particle polydispersity on activity is also discussed. Our work provides for the first time the link of processing (catalyst pretreatment), structure (nanoparticle size and shape), property (catalyst activity) relations for Ru catalysts used for ammonia decomposition, along with the optimum nanoparticle size.

2. Methods

2.1. Catalyst Synthesis. Supported Ru/Al_2O_3 catalysts were prepared using an incipient wetness technique. $\gamma\text{-}Al_2O_3$ was dried at 120 °C overnight prior to impregnation. A Ru nitrosyl nitrate solution ($Ru(NO)(NO_3)_3$) (Aldrich, 1.7 wt % Ru by weight) was used for most experiments (unless otherwise mentioned) and was added dropwise to the Al_2O_3 powder. The powder was shaken to ensure even distribution; then the powder was dried at 80 °C. The process was repeated until 4 wt % Ru loading was achieved. In order to investigate the effect of catalyst precursor, select results were also obtained (whenever explicitly mentioned) using a 4.5 wt % Ru/Al_2O_3 catalyst made via incipient wetness (same synthesis procedure as above) from a $Ru(acac)_3$ precursor (Aldrich).

Different aliquots of the as prepared catalyst were loaded into the reactor and subjected to the pretreatments summarized in Table 1. The first catalyst pretreatment (whether reduction or calcination) was done ex situ, and then 100 mg was weighed and added to 150 mg Al_2O_3 and subjected to subsequent pretreatment. The total gas flow rate was 200 sccm for all pretreatments, and the temperature ramp was 10 °C/min. Reductions and calcinations were performed in 10% H_2 in He and air, respectively. The hold time at the calcination and reduction temperatures was 1 h unless otherwise mentioned.

2.2. Catalyst Characterization and Activity Measurements. The kinetics of ammonia decomposition on Ru/Al_2O_3 catalyst was measured in a 1/4 in. stainless steel reactor at atmospheric pressure.

Table 1. Summary of the 4 wt % Ru/Al_2O_3 Catalyst Pretreatments Made from the Nitrosyl Nitrate Precursor

sample	first reduction temperature (° C)[a]	first calcination temperature (° C)	second reduction temperature (° C)
1	450	120	450
2	450	–	450
3	450	200	450
4	450	250	450
5	600[b]	350	450
6	–	500[c]	450
7	–	750[c]	450

[a] Ex situ. [b] 18 h. [c] Calcination (ex situ) for 5 h.

MKS calibrated digital mass flow controllers were used to control the flow rate of NH_3, H_2, N_2 and He. In order to eliminate temperature and concentration gradients, 100 mg of the catalyst powder was diluted with 150 mg inert Al_2O_3 of the same particle size (50−75 μm) and then packed in the reactor. The catalyst particle size and dilution were found to be sufficient to eliminate heat and mass transfer limitations (not shown). The difference in the temperature measured by three thermocouples (located near the entrance, at the middle, and near the exit of the bed) was less than 3 °C. The catalyst bed length was 1.9 cm. After the catalyst pretreatment, 10% NH_3 in He at 200 sccm total flow rate was introduced to the reactor, and NH_3 conversion was measured at different temperatures, starting from 450 °C and ramping down to 300 °C, to avoid sintering of the catalyst during the activity measurements. The reactor products were sampled with a gas-sampling valve, and the composition was monitored with a HP Series 6890 gas chromatograph (GC) using a thermal conductivity detector (TCD). The ammonia conversion was calculated using the H_2 and N_2 mole fractions in the products.

The exposed Ru surface area was measured by CO pulse chemisorption using an automated chemisorption analysis instrument from Altamira (AMI-200). After reactivity measurement, the catalyst was loaded into a 1/4 in. quartz tube. Prior to the pulse CO chemisorption measurement, the catalyst was reduced at 450 °C for 2 h in 10% H_2 (balance Ar) at 40 sccm total flow rate, then cooled down to room temperature in 30 sccm He. CO pulses were introduced to the sample (250 micro liters of 100% CO) and the CO uptake was measured using a TCD detector. The Ru dispersion was calculated assuming a CO:Ru stoichiometry of 0.6:1.[14,15]

Transmission electron microscopy (STEM and HRTEM) was performed on a JEOL 2010F FASTEM field emission scanning transmission electron microscope. The catalyst powder was dispersed in ethanol, and a sample was dropped on a carbon coated copper TEM grid. For detection of the very small Ru particles and estimation of particle size distributions, high angle annular dark field imaging (HAADF) was used in the STEM mode. Catalyst characterization (including EXAFS) was performed on the spent catalysts unless otherwise mentioned.

For the EXAFS analysis,[16] Ru/Al_2O_3 catalyst samples (after reactivity measurements) were pressed into self-supporting wafers and loaded in an in situ sample holder, then reduced at 450 °C for 1 h in pure H_2. The sample was cooled down to room temperature in pure H_2. Ru K edge EXAFS data for Ru/Al_2O_3 catalyst and a Ru foil located in a reference position were measured at room temperature simultaneously, in fluorescence and transmission modes, respectively, at beamline X18-B, National Synchrotron Light Source at Brookhaven National Laboratory. Details of the EXAFS data analysis are provided in the Supporting Information.

2.3. Microkinetic Modeling. Activity data were modeled using a comprehensive microkinetic model that does not employ any

(13) Honkala, K.; Hellman, A.; Remediakis, I. N.; Logadottir, A.; Carlsson, A.; Dahl, S.; Christensen, C. H.; Nørskov, J. K. *Science* **2005**, *307*, 555–558.
(14) Tsai, W.; Weinberg, W. H. *J. Phys. Chem.* **1987**, *91*, 5302–5307.
(15) Szmigiel, D.; Rarog-Pilecka, W.; Miskiewicz, E.; Kaszkur, Z.; Kowalczyk, Z. *Appl. Catal., A* **2004**, *264*, 59–63.
(16) Shu, Y.; Murillo, L. E.; Bosco, J. P.; Huang, W.; Frenkel, A. I.; Chen, J. G. *Appl. Catal., A* **2008**, *339*, 169–179.

assumptions about the rate-determining step or partial equilibration of any elementary-like reactions. The model simulates an isothermal fixed-bed reactor at steady state with conditions identical to the experimental ones. The elementary-like reactions are:

$$R_1{:}H_2 + 2* \underset{k_{1b}}{\overset{k_{1f}}{\rightleftharpoons}} 2H*$$

$$R_2{:}N_2 + 2* \underset{k_{2b}}{\overset{k_{2f}}{\rightleftharpoons}} 2N*$$

$$R_3{:}NH* + * \underset{k_{3b}}{\overset{k_{3f}}{\rightleftharpoons}} N* + H*$$

$$R_4{:}NH_2* + * \underset{k_{4b}}{\overset{k_{4f}}{\rightleftharpoons}} NH* + H*$$

$$R_5{:}NH_3* + * \underset{k_{5b}}{\overset{k_{5f}}{\rightleftharpoons}} NH_2*{+}H*$$

$$R_6{:}NH_3 + * \underset{k_{6b}}{\overset{k_{6f}}{\rightleftharpoons}} NH_3*$$

In the work described here, we use the DFT values for the activation energies at the B_5 sites[17] with minor modifications (ca. reactions R_{4f} and R_{5b}), and estimate the pre-exponentials of the elementary reactions subject to thermodynamic consistency using data of sample 6 (Table 1). Our model actually accounts for terrace sites, B_5 sites, or both (with diffusion of adsorbed species between terrace and B_5 sites in a thermodynamically consistent manner); however, as explained in the Results section, the terrace sites do not contribute to the catalyst activity. Hence, the discussion in later sections concentrates mainly on the model with only B_5 sites. The effect of adsorbate−adsorbate interactions on the activation energies was accounted for using bond-order conservation relations (through variation of the heat of chemisorption of nitrogen).[18] The strong effect of N (repulsive) adsorbate−adsorbate interactions on heats of chemisorption and activation energies, both through DFT calculations and experiments,[13,18] is well documented for the ammonia chemistry.

2.4. Density Functional Theory (DFT) Calculations of Structure Determination. In order to understand the effect of calcination, we constructed unsupported planar metallic Ru and Ru-oxide clusters of ∼0.5−1 nm in diameter and investigated their stability via DFT calculations. All calculations were carried out using the Becke−Perdew86 (BP86) functional,[19,20] the resolution of the identity (RI) approximation to the Coulombic energy, and the sv(p) basis set (default ECPs were included for the Ru atoms) as implemented in the Turbomole 5.9.0 program.[21] Select simulations on the effect of support are presented in the Supporting Information. The Ru and the Ru-oxide clusters were fully optimized without any symmetry constraints (structures shown in Supporting Information). We calculated the relative stability of the clusters in terms of the binding energy per atom (BE/n; n is the number of atoms in the cluster) from the following expressions:

$$\text{Metallic Ru}_n \text{ clusters:} \quad \mathrm{BE}/n = [E(\mathrm{Ru}_n) - n{\cdot}E(\mathrm{Ru})]/n$$

Here $E(\mathrm{Ru_n})$ is the total energy of the optimized $\mathrm{Ru_n}$ cluster, E(Ru) is the total energy of a Ru atom, and n is the number of Ru atoms of the $\mathrm{Ru_n}$ cluster.

$$\text{Ru-oxide clusters } (\mathrm{Ru}_x\mathrm{O}_y): \quad \mathrm{BE}/n = [(E(\mathrm{Ru}_x\mathrm{O}_y) - x{\cdot}E(\mathrm{Ru}) - y{\cdot}E(\mathrm{O})]/n$$

Here $E(\mathrm{Ru}_x\mathrm{O}_y)$ is the total energy of the optimized $\mathrm{Ru}_x\mathrm{O}_y$ cluster, E(Ru) and E(O) are the total energy of the Ru and O atom, respectively, and n is the total number of Ru and O atoms of the $\mathrm{Ru}_x\mathrm{O}_y$ cluster ($n = x + y$).

3. Results and Discussion

3.1. Catalyst Activity for NH_3 Decomposition. The catalyst pretreatment listed in Table 1 allowed us to vary the Ru dispersion from 95% to 5% corresponding to a Ru average particle size (from TEM) of 0.84 and 7.5 nm, respectively (Table 2). Figure 1 shows the effect of Ru dispersion and particle size on the catalyst (prepared from Ru nitrosyl nitrate precursor) activity for ammonia decomposition at 350 °C. The TOF [(moles NH_3 reacted/g_{cat}/s)/(moles Ru/g_{cat})] is obtained from the estimated rate normalized with the area per mass (the latter was measured via CO chemisorption; Table 2). The maximum TOF occurs at an average Ru particle size of ∼7 nm. Similar data were obtained at other temperatures (not shown). The optimal dispersion obtained herein is close to that in ammonia synthesis on Ru/C (10−15%).[7] However, the ∼7 nm optimal particle size is much larger than the 1.8−3.5 nm theoretically predicted in the literature[6,8,12] for reasons discussed below.

The activity of catalyst made from the $Ru(acac)_3$ precursor with the same treatment as sample 6 (Table 1) was also measured. This sample shows very similar dispersion and activity as sample 6, as shown in Figure 2. Our data indicate that these two catalyst precursors lead to the same catalytic activity when prepared in the same way.

3.2. Effect of Pretreatment on Particle Size and Shape. The effect of catalyst pretreatment (see Table 1) on Ru particles is summarized in Table 2. The average Ru particle diameter (d_{avg}) was obtained using TEM from the following correlation,

$$d_{\mathrm{avg}} = \sum_i n_i d_i / \sum_i n_i$$

where d_i is the particle diameter measured from STEM images scanning in the horizontal direction and n_i is the number of particles.[22]

Table 2 shows that the Ru dispersion decreases with increasing calcination temperature (sample 2 was subjected to a reduction pretreatment only). Figure 3 shows a representative STEM image of the spent sample 2 and the corresponding particle size distribution. Small, fairly round nanoparticles are seen; the same is true for sample 1, whose particle size distribution is also shown in Figure 3. The STEM image (sample 4) in Figure 4 shows larger rectangular-shaped particles as well as small, nearly round particles. The rectangular shape was dominant for larger particle sizes (e.g., samples 5−7) as revealed in Figure 5. The larger Ru particles showed lattice spacing of either the (011) or the (002) Ru crystallographic planes. No particles with lattice spacing corresponding to ruthenium oxide were detected, indicating that the Ru particles were not oxidized upon exposure to air after taking the catalyst out of the reactor. In addition, XRD data (see Supporting Information) of sample 6 indicated only metallic Ru. The average aspect ratio of the Ru particles in sample 6 was about 1.8.

Our results are consistent with the rectangular, flat particles observed by Song et al. in their study of Ru/HOPG (highly

(17) Logadóttir, Á.; Nørskov, J. K. *J. Catal.* **2003**, *220*, 273–279.
(18) Mhadeshwar, A. B.; Kitchin, J. R.; Barteau, M. A.; Vlachos, D. G. *Catal. Lett.* **2004**, *96* (1−2), 13–22.
(19) Becke, A. D. *Phys. Rev. A* **1988**, *38* (6), 3098–3100.
(20) Perdew, J. P. *Phys. Rev. B* **1986**, *33*, 8822–8824.
(21) Ahlrichs, R.; Bar, M.; Haser, M.; Horn, H.; Kolmel, C. *Chem. Phys. Lett.* **1989**, *162*, 165–169.
(22) Ertl, G.; Knözinger, H.; Weitkamp, J. *Handbook of Heterogeneous Catalysis*; VCH: Weinheim, 1997.

Table 2. CO Chemisorption and TEM Particle Size Results for Samples of Table 1.

catalyst sample no.	CO uptake (μmoles CO/g catalyst)[a]	Ru dispersion (%)[b]	TEM particle size (d_{avg}) (nm)
1	226	95	0.84
2	178	75	1.3
3	159	67	2.6
4	83	35	4.4
5	33	14	5.2
6	21	9	7.0
7	12	5	7.5

[a] CO uptake was measured on the spent catalyst. [b] Assuming 4 wt % Ru loading.

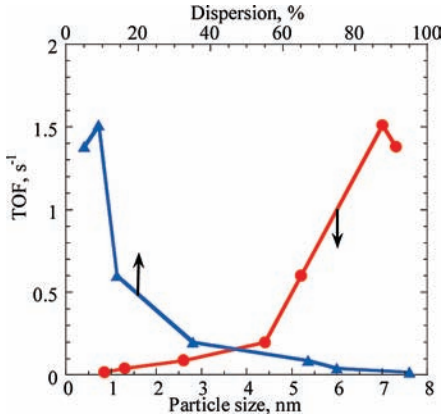

Figure 1. Turnover frequency for NH_3 decomposition at 350 °C and 1 atm as a function of Ru particle size (circles) and Ru dispersion (triangles). Total flow rate = 200 sccm, 10% NH_3 in He, 100 mg 4 wt % Ru/Al_2O_3 (from Ru nitrosyl nitrate) diluted with 150 mg Al_2O_3. The lines connect the points.

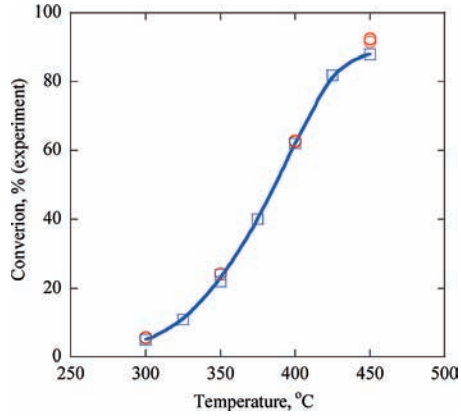

Figure 2. Conversion vs temperature comparing two catalysts prepared from the nitrosyl nitrate (circles) and $Ru(acac)_3$ (squares) precursors using the same pretreatment (that of sample 6). Both the dispersion and the conversion of the two samples are nearly the same. The line just connects the points. Total flow rate = 200 sccm, 10% NH_3 in He, P = 1 atm.

oriented pyrolytic graphite) model catalysts using scanning tunneling microscopy (STM)[10] and by Datye et al. in their HRTEM study on Ru/MgO.[23] Song et al. reported particles as wide as 50 nm with only 3 nm height and a high density of steps at this high aspect ratio.[10]

To complement the information obtained using TEM and CO chemisorption, some of the catalyst samples were further characterized using EXAFS (see Supporting Information). Table

(23) Datye, A. D.; Logan, A. D.; Long, N. J. *J. Catal.* **1988**, *109*, 76–88.

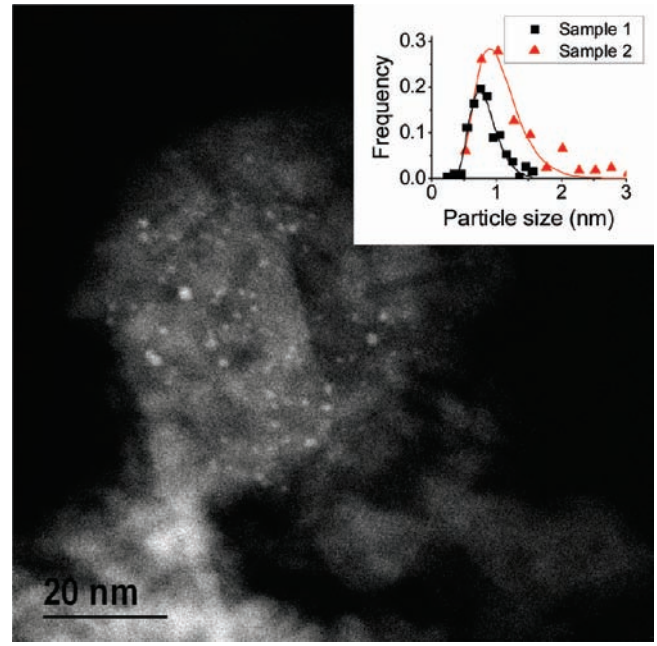

Figure 3. HAADF STEM image of the 4 wt % Ru/Al_2O_3 sample 2 (spent). The inset shows particle size distribution of samples 1 (squares) and 2 (triangles). The number of particles measured from STEM images was 170 and 190, respectively. The number average from STEM (d_{avg}) was 0.84 and 1.3 nm, respectively. The solid lines are log-normal distribution fits of samples 1 and 2 with an average of 0.8 and 1 nm, respectively.

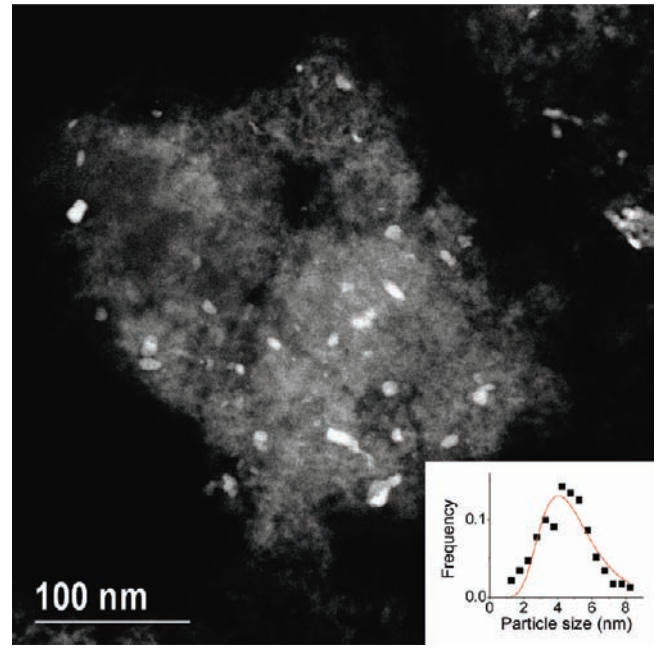

Figure 4. HAADF STEM image of the 4 wt % Ru/Al_2O_3 sample 4 (spent). Several large-size particles with elongated shape along with much smaller particles are seen. The inset shows the particle size distribution. The number of particles measured from STEM images was 280. The number average from STEM (d_{avg}) was 4.4 nm. The solid red line is a log-normal distribution fit with an average of 4.6 nm.

3 shows the results from the EXAFS analysis for the Ru foil (bulk standard) and catalyst samples 1, 3, and 6. The average coordination numbers of the first four shells fitted for the Ru foil show that our model is accurate in determining the first, second and fourth shell coordination numbers, while it highly underestimates the third. However, the uncertainty in the fitted

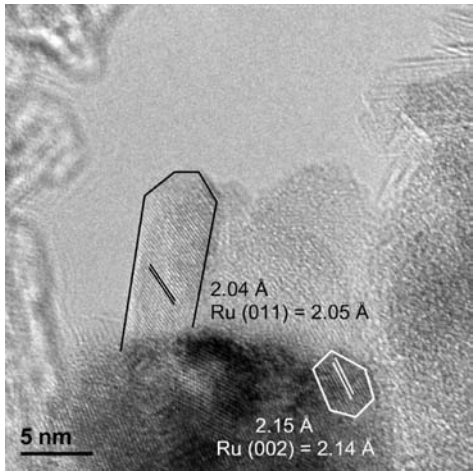

Figure 5. HRTEM image of sample 6 (spent) showing an elongated rectangular-shaped particle (left) and a more isotropic particle (right).

Table 3. EXAFS Results for Select Samples of Table 1[a]

coordination	Ru bulk	foil	sample 1	sample 3	sample 6
1NN	12	12.4 (0.7)	3.3 (0.6)	5.2 (0.5)	10 (0.7)
2NN	6	6.1 (2.1)	–	2.5 (1.8)	6.7 (2.5)
3NN	18	11.5 (3.3)	–	5.3 (4.1)	9.2 (3.1)
4NN	12	10.7 (5.5)	–	0.4 (0.9)	8.1 (4.5)

[a] *i*NN indicates the i^{th} nearest neighbor.

value for the fourth shell coordination number is high, indicative of low sensitivity to this coordination number. Therefore, only the average coordination numbers of the first two shells are used for extracting information for the particle shape of the Ru/Al_2O_3 samples.[24]

The EXAFS data for the Ru/Al_2O_3 samples, plotted in *r*-space by Fourier transforming the k^2-weighted data in the same *k*-range from 2 $Å^{-1}$ to 17 $Å^{-1}$, was compared with the Ru foil data that features peaks characteristic of the close-packed (specifically, hcp) crystal structure of the Ru metal. The data revealed the presence of close-packed Ru nanoparticles in all the samples (Figure 6a). The Fourier transform of the Ru/Al_2O_3 catalysts shows that the Ru particles are metallic, with bonding environments similar to those found in the Ru bulk (foil). Figure 6b shows the Fourier transform magnitudes of the data for sample 3 along with the best fit up to 5.42 Å in *r*-space. The nine-photoelectron scattering paths included in our model (single- and multiple-scattering ones) (details in Supporting Information) accurately reproduced the data for the first four shells, as shown in Figure 6b. Good agreement was also obtained for the other Ru/Al_2O_3 model fits (Figure 2 in Supporting Information).

For the smallest nanoparticles (sample 1), only the first shell coordination number was fitted (since the more distant shells could not be resolved), consistent with the fact that the Ru particles were very small. The Ru particle size and shape can be reconstructed using the coordination number obtained from EXAFS. A first shell coordination number of 3.2 ± 0.7 corresponds to a monolayer structure of 9−15 atoms. The smallest bilayer cluster of a hexagonal crystallographic structure, shown in Figure 7a, consists of 10 atoms and has an average first shell coordination number of 4.8, which is higher than that

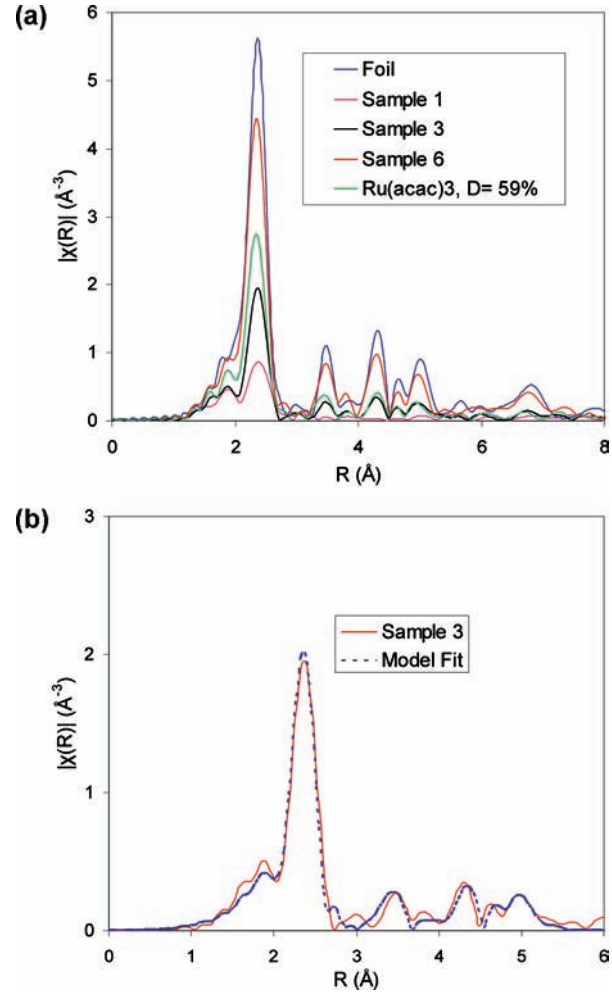

Figure 6. (a) Fourier transform magnitudes of k^2-weighted $\chi(k)$ data for the K edge EXAFS spectra of the Ru foil and the Ru/Al_2O_3 catalysts. (b) Fourier transform magnitudes of the data and multiple scattering fit for the Ru/Al_2O_3 (sample 3) catalyst.

of the EXAFS data. Figure 7b shows a possible flat structure with an average first shell coordination number of 3.7 and a diameter (average of length and width) of 0.64 nm. The structural characteristics of this shape are close to the EXAFS results and the TEM average diameter of 0.84 nm, and consistent with the very high dispersion (∼95%) estimated from CO chemisorption.

Analysis of the EXAFS data for samples 3 and 6 was more challenging. Figure 1 in the Supporting Information shows the average first shell coordination number for hemispherical hcp particles vs particle diameter. The average first shell coordination number for samples 3 and 6 differs greatly from those of hemispherical particles of a similar average diameter. For example, sample 3 of an average particle size of $d_{avg} = 2.6$ nm corresponds to an average first shell coordination number of ∼9.5 (Supporting Information, Figure 1), which is much larger than the EXAFS coordination number of 5.2 (Table 3).

For particles in the diameter range of 2−3 nm (e.g., sample 3), the number of possible shapes with low average first and second shell coordination numbers (comparable to EXAFS results) is high. These low coordination numbers imply that the particles should be 2−3 layers high with two or more steps per particle (Figure 8). The average coordination numbers for the first and second shells of the particles (see caption of Figure 8)

(24) Frenkel, A. I.; Hills, C. W.; Nuzzo, R. G. *J. Phys. Chem. B* **2001**, *105*, 12689–12703.

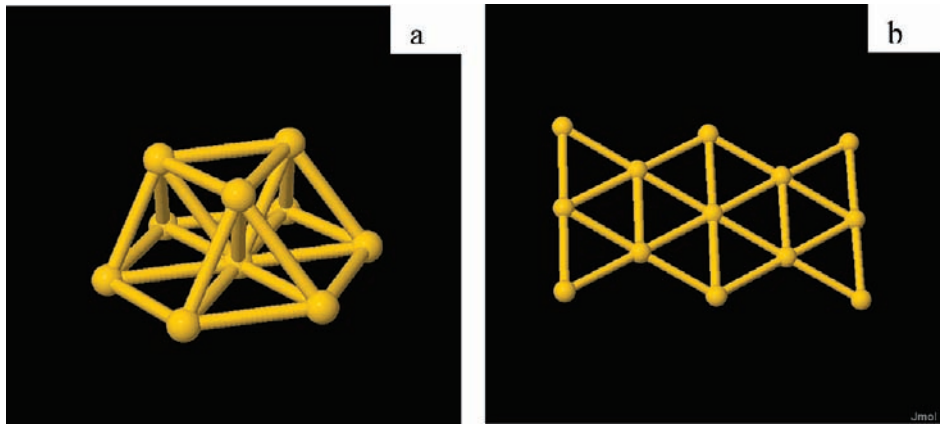

Figure 7. Possible Ru particle shapes for sample 1 (experimental data: $d_{avg} = 0.84$ nm, first shell coordination number = 3.3). (a) Two-layer Ru structure with 0.48 nm diameter and first shell coordination number of 4.8.(b) One-layer Ru structure with 0.94 nm length, 0.52 nm width, and a first shell coordination number of 3.7.

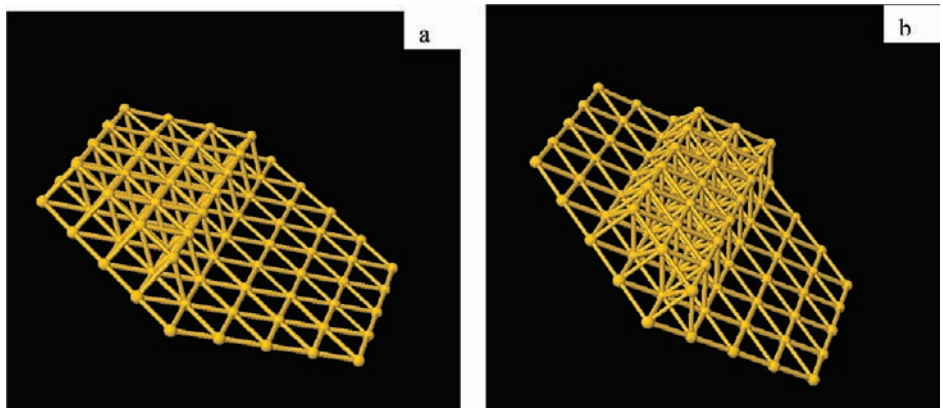

Figure 8. Possible Ru particle shapes for sample 3 (experimental data: $d_{avg} = 2.62$ nm, first and second shell coordination numbers 5.2 and 2.5, respectively). (a) Two-layer Ru structure with one step, a diameter = 2.12 nm, and first and second shell coordination numbers of 6.5 and 1.5, respectively. (b) Two-layer Ru structure with two steps, a diameter = 2.12 nm, and first and second shell coordination numbers of 6.4 and 1.5, respectively.

differ from those obtained using EXAFS (Table 3). This is likely due to the broad particle size distribution of this sample (not shown), which makes the interpretation of coordination numbers difficult. In order to illustrate this point, we consider for simplicity that the coordination numbers are the result of averaging over two types of particles. The first type consists of small, one layer flat clusters, such as the one in Figure 7b, and the second type consists of larger particles (2−3 nm in diameter) with one to two steps per particle, as shown in Figure 8. If we assume that 95% of the particles are of the first type and only 5% are of the second type, the average first shell coordination number (averaged over the total number of atoms to account for the larger mass for the bigger particles) would be about 5, in good agreement with the experimentally obtained value of 5.2. Estimation of the number of B_5 sites for this distribution, assuming one step per particle for the larger particles (5% of the distribution), would be on the order of 20−30 B_5 sites per 100 particles (4−6 B_5 sites per large particle), which corresponds to 0.7−1% of the surface sites being B_5 sites (number of B_5 sites divided by the total number of surface atoms). Further evidence for particle polydisperisty and its effect on activity is provided from modeling the activity measurements (see below).

Figure 9 shows a possible shape for the larger particles (sample 6). The first and second shell average coordination numbers are 10.7 and 5, respectively, which are in close agreement with the experimentally obtained values (Table 3).

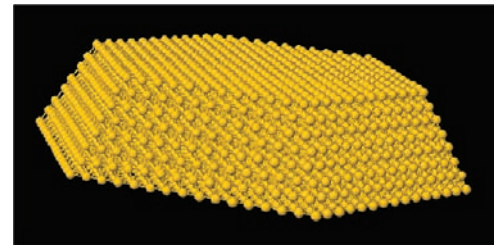

Figure 9. Possible Ru particle shape for sample 6 with diameter = 7.6 nm, height = 1.5 nm, and first and second shell coordination numbers of 10.7 and 5, respectively. Corresponding experimental values: $d_{avg} = 7$ nm, EXAFS first and second shell coordination numbers of 10, and 6.7, respectively.

The aspect ratio (diameter/height) of the particle is high (about 5), which is in agreement with HRTEM (Figure 5). The dispersion of the particle shown in Figure 9 is about 19%, which is in reasonable agreement with the 9% dispersion measured via CO chemisorption. We estimate a range for the number of B_5 sites assuming two cases of steps between the (011) and (001) planes. The first case is when the step is along the perimeter on the top of the particle, with one row of atoms being removed on each edge of the hexagon. The second case is when a step is formed every two layers in the (001) direction, which results in three steps on the sides of the particle. These structures

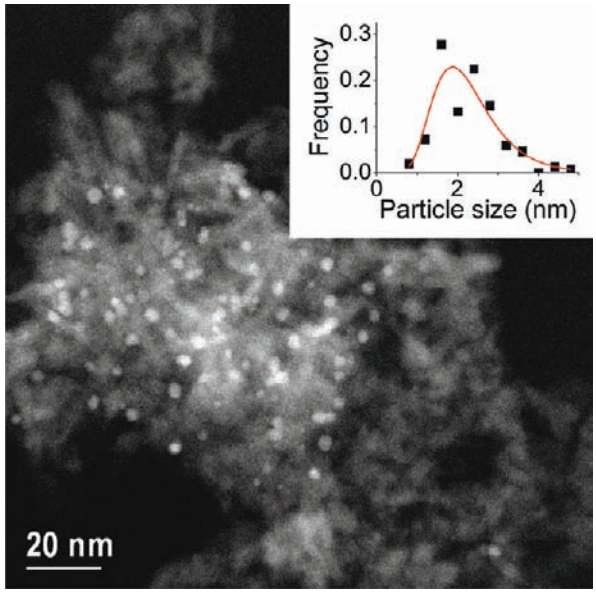

Figure 10. HAADF STEM images of 4.5% Ru/Al_2O_3 catalyst prepared from $Ru(acac)_3$. The catalyst was reduced at 450 °C without any calcination. Image taken after activity measurements for NH_3 decomposition. Round-shaped particles are also seen. The dispersion was 59% and d_{avg} from TEM was 2.2 nm.

correspond to 4% and 12% of the surface sites being B_5 sites for cases 1 and 2, respectively. These are rough estimates, since the average first shell coordination number is not sensitive to steps at this large particle size. Simple geometric arguments indicate that a flat particle would have more step sites than a hemispherical particle of the same diameter. This is due to the larger top layer surface/perimeter of the flat particle.

In order to put our work in context with literature and assess the effects of pretreatment, a sample was prepared from the $Ru(acac)_3$ precursor and pretreated as sample 2 (see Table 1). The Ru particles are 2.2 ± 0.7 nm in diameter (Figure 10) and have a first shell coordination number of 7.7 ± 0.5 (compared to 5.2 for sample 3 of a similar Ru particle size), which is close to 8.6 for a 2 nm hemispherical particle (Figure 1 in Supporting Information). Comparison of different catalyst pretreatments provides strong support that the elongated, flat shapes result from calcination, whereas reduction alone results in a hemispherical shape. The latter shape is consistent with HRTEM images on Ru/magnesium−aluminum spinel catalyst (synthesized from the same nitrosyl nitrate precursor we used) that was not subjected to calcination.[8] We believe that the flat Ru particle shapes observed herein are mainly a result of the catalyst pretreatment and not of roughening from N_2/NH_3 during reaction. This is supported by the work by Song et al., where a high density of steps was observed on flat Ru particles without exposure to NH_3 or N_2.[10]

3.3. Insights into the Effect of Calcination and Support on Particle Structure. DFT calculations on unsupported metallic and oxide clusters starting from initially flat structures revealed that metallic small Ru clusters easily form 3D structures rather than maintaining their (initial) planar structure (see Figure 11b for examples and Supporting Information for all clusters studied and coordinates). The mean coordination number (mCN) of the metal atoms in the 3D structures is higher compared to that of the planar ones. In the case of the oxides, many clusters can be stabilized in planar forms, especially in oxygen-rich cases. Figure 11 compares the relative stability of the metallic Ru and Ru-oxide clusters and shows the structures of some representative ones (metallic Ru_9, Ru_{11}, Ru_{12}, and their oxides). It is clearly shown that the presence of O atoms in the Ru cluster stabilizes by approximately 25 kcal/mol (per atom) the structures compared to the metallic ones (Figure 11a). In addition, Figure 11b shows that candidate planar Ru structures (according to our EXAFS and TEM analysis), such as the Ru_9, Ru_{11} and Ru_{12}, can only be stabilized in their oxide form. The diameters of the Ru_9, Ru_{11}, and Ru_{12} oxide clusters are in the range of 0.6−0.8 nm and the mCN's of the Ru atoms are 2.7, 3.6, and 4.0, respectively. The structure and coordination number of Ru_{11} are similar to those postulated in Figure 7b for Ru_{13}. The Ru_{11} (as well as several other clusters shown in the Supporting Information) has a coordination number that is in good agreement with the EXAFS data of sample 1 (Table 3). Select simulations on supported clusters (Supporting Information) indicate that while the support has a secondary effect on cluster structure (the oxygen from the support may partially stabilize a flat shape of very small clusters), an oxygen-rich environment is key to stabilization of flat structures, consistent with the calculations of unsupported clusters. Our calculations indicate that upon calcination, Ru forms planar oxide structures, and these structures are stable on the support during catalyst reduction.

3.4. Modeling of Activity: Importance of Shape and Polydispersity. In order to extract quantitative information on the fraction of active (B_5) sites and understand the effect of shape on activity, a microkinetic model for ammonia decomposition was developed. The pre-exponentials of the microkinetic model were refined using data for sample 6 (see Methods). The model parameters are shown in Table 4; 95% confidence intervals on pre-exponential factors (excluding sticking coefficients) are approximately 10^7.

The model is assessed against data on catalysts of varying dispersion. The kinetic data include studies of the effect of temperature and feed-flow rate on the steady-state conversion of ammonia, as well as the effect of inhibition by cofeeding hydrogen and/or nitrogen along with ammonia, with nearly 200 data points collected on catalysts of varying Ru dispersion. The only parameter estimated in describing the activity of catalysts of different dispersion (aside from sample 6) is the number of active sites. The results are shown in Figure 12. The model describes the data very well for catalysts of varying dispersion. To our knowledge, this is the first fully quantitative, first-principles based, complete microkinetic model for the ammonia decomposition chemistry on Ru catalyst that explicitly considers kinetic information for step and terrace sites, and integrates it with the fractions of step and terrace sites.

Other microkinetic models in the literature, e.g.,[18,25] rely on the average behavior of catalyst surface atoms to deduce kinetic parameters from empirical methods or experiments. Consequently, such models would likely require different kinetic parameters to describe the activity of catalysts of different size and shape. Norskov and co-workers considered steps as the active sites but did not build a full microkinetic model.[13] Based on our combined B_5 and terrace model, terrace sites do not contribute to the catalyst activity, in agreement with literature.[11,26] On step sites, the most abundant reactive intermediate (MARI) is predicted to be adsorbed NH_3 at lower temperatures and

(25) Hinrichsen, O. R., F.; Muhler, M.; Ertl, G. *Chem. Eng. Sci.* **1996**, *51*, 1683–1690.
(26) Dahl, S. L., A.; Egeberg, R. C.; Larsen, J. H.; Chorkendorff, I.; Törnqvist, E.; Nørskov, J. K. *Phys. Rev. Lett.* **1999**, *83*, 1814–1817.

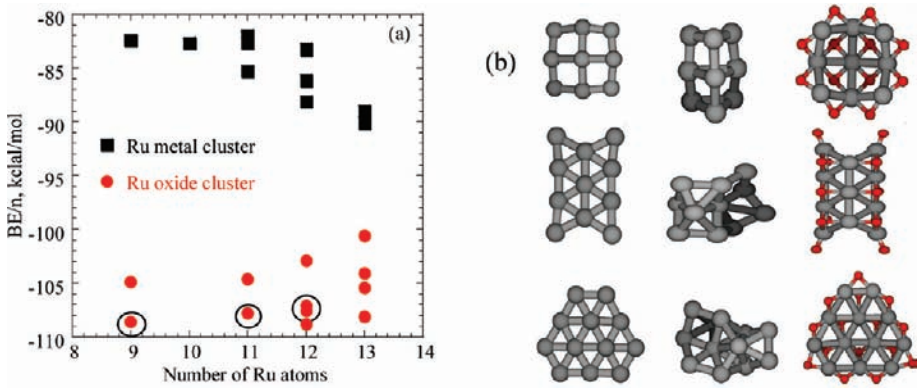

Figure 11. (a) Relative stability of Ru clusters (black squares) and Ru-oxides (red filled circles). (b) Initial planar structures of metallic Ru_9, Ru_{11}, and Ru_{12} clusters (left column), fully optimized (3D) metallic structures (middle column), and their fully relaxed planar oxides (right column). The open circles in panel (a) correspond to the oxides shown in (b).

Table 4. Parameters of the B_5 Active Site Based Microkinetic Model

reaction	pre-exponential (s^{-1}) or sticking factor (unitless)	activation energy (kcal/mol)
R_{1f}	7.73×10^{-4} [a]	0.0
R_{1b}	2.50×10^{12}	24.6
R_{2f}	2.41	$9.2 + 26.2\ \theta_N$ [b]
R_{2b}	1.18×10^{15}	$27.7 - 43.7\ \theta_N$
R_{3f}	6.40×10^{14}	$24.7 + 15.7\ \theta_N$
R_{3b}	1.58×10^{15}	$25.1 - 19.3\ \theta_N$
R_{4f}	1.10×10^{16}	29.8
R_{4b}	4.99×10^{14}	31.0
R_{5f}	2.62×10^{9}	20.5
R_{5b}	3.81×10^{16}	24.5
R_{6f}	0.279 [a]	0.0
R_{6b}	6.55×10^{13}	20.0

[a] Sticking coefficient. [b] θ_N is the nitrogen coverage.

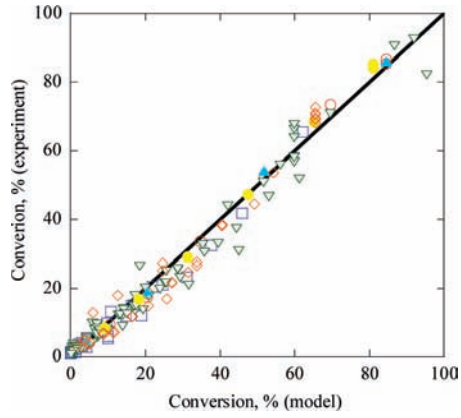

Figure 12. Parity plot of (microkinetic model) predicted conversion of ammonia against experimental conversion. The model was refined on data for the 9% dispersion catalyst. Nearly 200 experimental points were measured for various temperatures, flow rates, and feed compositions (different symbols indicate data sets from catalysts of varying dispersion). The average relative error of model predictions is approximately 12%. Note that 95% confidence intervals on the pre-exponential factors specified in Table 4 (except sticking factors) are approximately 10^7. All experiments were conducted at atmospheric pressure.

adsorbed H at other conditions. The rate-determining step (RDS) for most conditions considered is the dehydrogenation reaction ($NH_2^* + * \leftrightarrow NH^* + H^*$), and N_2 adsorption/desorption is also RDS at a significant number of conditions.

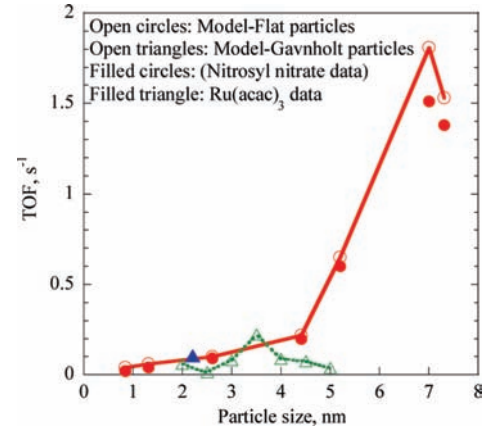

Figure 13. Turnover frequency (TOF) in (moles NH_3 reacted/g_{cat}/s)/(exposed moles Ru/g_{cat}), for NH_3 decomposition at 350 °C and 1 atm as a function of Ru particle size. Experimental data in filled circles and microkinetic model in open circles for the nitrosyl nitrate catalyst. Total flow rate = 200 sccm, 10% NH_3 in He, 100 mg of 4 wt % Ru/Al_2O_3 diluted with 150 mg Al_2O_3. For comparison, the measured TOF for the $Ru(acac)_3$ precursor catalyst with dispersion $D = 59\%$ (filled triangle; pretreatment similar to sample 2) and the predicted TOF using the fraction of B5 step sites predicted by Gavnholt and Schiøtz (open triangles; see text) are also shown.

Figure 13 compares the experimental (filled circles) and model-based (open circles) TOF as a function of particle size for the nitrosyl nitrate catalyst. The model captures the experimental data very well. The slight deviation between model and experimental TOFs (e.g., at the lowest dispersions considered) is due to the fact that the model is refined using a large kinetic data set for sample 6, and has not been fitted solely to the data points of Figure 13. The estimated percent of B_5 sites, using data from Figure 13, is given in Figure 14 (circles), and is in reasonable agreement with the aforementioned characterization results, providing further support for the proposed (flat) Ru particle structures.

Theoretical estimates (mentioned in the introduction) suggest that the optimum particle size to achieve the highest TOF for NH_3 decomposition for hexagonal Ru particles is 1.8−3 nm. This size is quite different from the one for flat nanoparticles obtained herein. The estimated (from the geometry) fraction of B_5 sites of hexagonal particles[6,8] (with height approximately equal to the width) vs dispersion is also shown in Figure 14 (dotted line). It is clear that a maximum

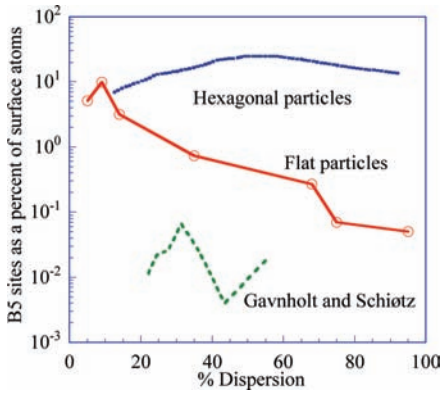

Figure 14. B_5 sites as a percent of total surface sites vs the (percent) catalyst dispersion estimated via microkinetic model analysis of experimental data (circles; samples 1−7 in Tables 1 and 2), from the geometric shape of hexagonal particles (blue, dotted line), and from the simulated structures of Gavnholt and Schiøtz (green, dashed line).

fraction of B_5 sites is attained for dispersion of 50−60%, much higher than the ∼9% for flat nanoparticles. In their recent computational work, Gavnholt and Schiøtz indicated that the fraction of step sites in fcc/hcp-like particles should be significantly lower than simple geometric counting,[12] as shown in Figure 14 (dashed line). It is clear that our smallest nanoparticles have a comparable fraction of B_5 sites (of the total surface atoms) as those predicted by Gavnholt and Schiøtz. In contrast, our larger particles exhibit many more step sites than regular fcc-/hcp-like particles. It will be desirable in future work to be able to predict from first principles the effect of synthesis conditions on particle shape and on the fraction of active sites instead of estimating this from experimental data (in our case via microkinetic modeling). In addition, probe characterization, e.g., via STM, could independently provide an assessment on the type of steps and sites that may be responsible for the observed activity and interrogate modeling results. These approaches could provide invaluable, detailed input (well beyond average chemisorption studies) for microkinetic models.

In order to elucidate the effect of shape on activity, we have used the microkinetic model developed above and the fraction of B_5 sites from the theoretical work of Gavnholt and Schiøtz.[12] The predicted TOF is shown in Figure 13 (open triangles). A clear maximum at ∼3.5 nm is observed, confirming previous literature hypothesis. The predicted TOF is of the same order of magnitude as the smaller round particles made from the nitrosyl nitrate precursor (sample 2) and the $Ru(acac)_3$ precursor ($D = 59\%$) without calcination, indicating that the theoretical prediction provides a much more reasonable atomistic structure than step counting based on an assumed geometric shape. It becomes also apparent that the fraction of B_5 sites on flat-like particles exhibits much higher sensitivity with particle size than that of hexagonal-like and fcc-/hcp-like particles. As a result, the activity variation is also more dramatic. It should also be noted that the maximum activity per gram Ru (not only the TOF) is higher on the 7 nm flat-like particles compared to the 3 nm fcc/hcp (hemispherical) particles, indicating a higher number of B_5 sites per gram Ru on the flat particles despite their much lower dispersion. Furthermore, our results are qualitatively consistent with those of Song et al. who found that flat Ru particles of rectangular shape (as long as 50 and 3 nm in height) had a much higher activity for nitrogen adsorption.[10] On the basis of the characterization studies presented above, we attribute the increase in activity with increasing Ru particle size to the much higher number of B_5 sites available on the larger, flat-shaped Ru particles.

It is possible that other active sites also contribute to the catalyst activity. Gavnholt and Schiotz indicated that three additional types of sites may be active in the ammonia reaction;[12] most of these sites have similar activity as the B_5 site. Since a kinetic model based on B_5 sites alone along with the calculated surface fractions of these sites explains the behavior of a series of catalysts of different shapes and sizes without modification of any parameters of the model, this provides strong support that B_5 sites are representative of all the important active sites for this system. With the current experimental data, the microkinetic model cannot distinguish small differences among different types of step sites.

Finally, as noted earlier, terrace sites provide no contribution to the catalyst activity. A microkinetic model consisting only of flat, single layer small nanoparticles (e.g., see Figure 7b) shows no measurable activity. The lack of activity of the single layer nanoparticles provides further evidence of the characterization results (section 3.2) that point to the importance of polydispersity of small nanoparticles not only in matching the coordination numbers of EXAFS data but also in understanding the activity of very small particles (Figures 12 and 13). In other words, the data indicate that the (albeit low) activity of small nanoparticles (average diameter <1.5 nm; samples 1 and 2) is probably due to the presence of a very small fraction of larger nanoparticles that have B_5 sites, rather than the single layer nanoparticles themselves.

4. Conclusions

We studied the effect of Ru particle size and shape on the activity of $Ru/\gamma\text{-}Al_2O_3$ catalysts for ammonia decomposition via activity measurements, multiple characterization methods, and first-principles microkinetic modeling. Our results clearly showed that ammonia decomposition on Ru is highly structure sensitive, with TOF values increasing by almost 2 orders of magnitude as the particle size increases from 0.8 nm to >7 nm. We demonstrated for the first time that data from TEM, gas chemisorption and EXAFS can be combined to provide consistent structural models of the particle shape. This combined analysis allowed us to show that the Ru particle shape changes with increasing particle size from round ones (small particles) to flat, elongated ones (large particles) and to estimate the fraction of B_5 sites. Experiments and first-principles simulations indicate that catalyst calcination is key to controlling particle shape and giving rise to flat Ru nanoparticles. A complete microkinetic model was constructed to describe, for the first time, activity−size/shape data quantitatively. The model was employed to estimate the fraction of active (B_5) sites and provided further evidence in support of the characterization results. Our modeling results provided evidence that the (low) catalyst activity measured for small nanoparticles is most probably arising from particle size polydispersity (a small fraction of large particles) rather than activity on terraces. To our knowledge, this is the first indication of (unusual) invisibility of particles (due to their small fraction rather than their small size), which is at the other extreme of recent studies (e.g., in Au catalysis) where very small clusters, which are below the HRTEM resolution ('invisible'), are the most active. Future work on controlling

dispersion and measuring its effect on activity as well as on more detailed, microscopic characterization of the active sites, e.g., using STM, will be interesting. In addition, understanding the kinetics of nanoparticle formation will be essential in linking synthesis with structure and catalyst properties. Our results may be relevant to other reactions exhibiting maximum TOF at a certain particle size and indicate that along with dispersion or microscopy measurements, it is important to determine the particle shape in order to develop quantitative particle size/shape−activity relations.

Acknowledgment. We acknowledge financial support from the U.S. Department of Energy (DE-FG02-06ER15795). Use of the National Synchrotron Light Source, Brookhaven National Laboratory, for the EXAFS experiments was supported by the U.S. Department of Energy (DE-FG02-05ER15688).

Supporting Information Available: EXAFS analysis, XRD data, and the DFT results. This information is available free of charge via the Internet at http://pubs.acs.org.

JA902587K